Enhanced inner-shell x-ray emission by femtosecond-laser irradiation of solid cone targets

XiaoYa Li,[1,*] JiaXiang Wang,[2] WenJun Zhu,[1,†] Yan Ye,[1] Jun Li,[1] and Yong Yu[1]
[1]*National Key Laboratory of Shock Wave and Detonation Physics, Mianyang, 621900 Sichuan, China*
[2]*State Key Laboratory of Precision Spectroscopy, East China Normal University, Shanghai 200062, China*
(Received 8 August 2010; revised manuscript received 6 December 2010; published 18 April 2011)

The possibility of enhancing inner-shell x-ray emission, especially $K\alpha$ emission, by femtosecond-laser irradiation of solid cones instead of foils was investigated theoretically. In a model for hot electron (HE) transport and $K\alpha$ x-ray generation, $K\alpha$ emission from laser-irradiated solid cones and foils is investigated. As a complementarity to the model, the contributions from electric and magnetic fields generated by the HE current in solid cones and foils are discussed. The results indicate that the efficiency of HE energy conversion to $K\alpha$ photons is improved and the optimum HE temperature is increased.

DOI: 10.1103/PhysRevE.83.046404 PACS number(s): 52.25.−b, 52.65.Rr

I. INTRODUCTION

Inner-shell x-ray emission, especially $K\alpha$ radiation, from targets subjected to ultrashort laser irradiation is widely used for detection of warm dense matter, plasmas, and shock-compressed materials [1–3]. Improved brightness for this type of emission can be achieved by increasing the absorption rate of hot electrons (HEs) to the laser energy using laser pulse control [4,5], target surface treatment [6,7], or a suitable choice of a dense material [8,9]. For foil targets, optimal foil thickness and HE temperature (or laser intensity under a certain mechanism of laser-plasma interaction) are required in order to increase the efficiency of HE energy conversion to $K\alpha$ x-ray photons [10,11]. Beyond the optimal laser intensity, experiments showed that the brightness of $K\alpha$ emission does not increase with the increase of laser intensity [12,13]. Consequently, increased energy of the incident laser does not result in increased brightness of $K\alpha$ emission from foils, unless one increases the focus diameter of the laser, which results in an increase of the source size.

In this work we propose that a configuration of the target shape to reduce x-ray losses while maintaining HE transport within the target would enhance the efficiency of HE energy conversion to $K\alpha$ photons and increase the optimal laser intensity. A solid cone is one of the alternatives, which is easy to produce and allows repetitious irradiation. Unlike the reentrant cones introduced in inertial confinement fusion (ICF) research [14–16], which increase HE temperature and $K\alpha$ fluorescence through optical guiding of the laser pulse with intensity higher than 10^{19} W/cm^2 and produce prominent fast electron flow at the tip, the solid cones work at lower laser intensity, about $10^{17} \sim 10^{19}$ W/cm^2, as seen later, and the number of HEs emitted at the tip is minimized. Therefore, a solid cone target should be a good substitute for the foil target as the x-ray source induced by tabletop lasers.

To prove this idea, $K\alpha$ emission from solid cones vs foils is calculated in this paper. There has been a series of models for $K\alpha$ emission calculation [10–12,17]. The ITS Monte Carlo code is widely used to simulate HE transport and photon generation [18]. However, all the models are restricted to foil targets in which the electric and magnetic fields generated by HE currents are ignored. ITS 5.0 is capable of simulating HE transport in targets with complex geometry [19], but a solid cone target is not considered. In this work a model for HE transport and $K\alpha$ emission is introduced, and then contributions from static electric and magnetic fields generated in foils and solid cones are discussed.

The paper is organized as follows. In Sec. II, the calculation model for $K\alpha$ emission of solid cones and foils irradiated under a femtosecond high-power laser is introduced. In Sec. III, the results of $K\alpha$ emission from solid cones and foils are obtained, and the dependence of $K\alpha$ emission on the shape of the cone target and the temperature of HEs, or laser intensities when the absorption mechanism is determined, are studied. In Sec. IV, the electric and magnetic fields are estimated and their contributions to HE transport and $K\alpha$ generation are discussed. Section V is the conclusion.

II. MODELING

For laser-irradiated solids or other materials, when a $1s$ vacancy exists due to impact ionization of the atom by high-energy electrons, there is a possibility for an L-shell $2p$ electron or an M-shell $3p$ electron transiting to the K-shell $1s$ state, resulting in $K_{\alpha/\beta}$ radiation or an Auger electron. Similarly, L radiations are the result of transitions to the L-shell vacancy. In the manuscript we calculate only $K\alpha$ emission, with the difference between $K_{\alpha 1}$ and $K_{\alpha 2}$ (corresponding to transitions $2p_{3/2} \rightarrow 1s$ and $2p_{1/2} \rightarrow 1s$, respectively) ignored. The target is considered to be copper. The focus diameter of the laser pulse is considered to be $d = 20\ \mu$m, the half duration $\tau = 50$ fs, and the intensity I is varied from 10^{15} W/cm^2 to 2×10^{19} W/cm^2. In the following, we first discuss the HEs produced during laser-solid interaction and then simulate the transport of these HEs and calculate the number of $K\alpha$ photons emitting from the target.

We assume that HEs are generated on the surface over a spot with diameter d coinciding with the laser focus spot and that they obey an exponential energy distribution [20–22]

$$f(E) = \frac{1}{T_h}\exp(-E/T_h), \tag{1}$$

*xylapril@gmail.com
†wjzhu@caep.ac.cn

where E is the HE kinetic energy, and T_h is the HE temperature in kiloelectronvolts. When resonance absorption dominates, T_h is related to laser intensity I as [21,23,24]

$$T_h = 100\left(\frac{I\lambda^2}{10^{17}\,\mathrm{W\,cm^{-2}}\mu\mathrm{m}^2}\right)^{1/3}\ \mathrm{keV}. \quad (2)$$

When ponderomotive force dominates, the $T_h \sim I$ relation scales as [20]

$$T_h = m_0c^2\left[\left(1+\frac{I\lambda^2}{1.37\times10^{18}\,\mathrm{W\,cm^{-2}}\,\mu\mathrm{m}^2}\right)^{1/2}-1\right], \quad (3)$$

where m_0 is the static mass of electron. The direction of HEs into the target is assumed to be at divergence angle θ [Fig. 1(a)]. Particle-in-cell (PIC) simulation and the related analysis in Ref. [25] have shown that the ejecting angle of individual electrons is 0° for normal incidence of lasers and is in the range from 0° to the incident angle for oblique incidence, and the lower energy electrons have a lower ejecting angle. In our calculation, the results for $\theta = 0°$ are considered explicitly and those for $\theta = 20°$ are calculated as a comparison. In the following, the dependence of $K\alpha$ emission on T_h is calculated through simulating the transport of HEs in solid cone targets compared to that in foil targets, and the dependence of $K\alpha$ emission on laser intensity is discussed while resonance absorption or ponderomotive force dominates.

During transport, the electrons scatter with cold atoms, losing energy and producing $K\alpha$ emission, which is measured 1 mm from the target center at angle β (0° ~ 180°), as is shown in Fig. 1(a). The detector area is 1 μm^2. The cone is divided into disks of thickness dr, each disk is divided into circles of width dr, and each circle is divided into arcs of length dr [Fig. 1(b)]. The photon number measured at detector $D(x,y,z)$ produced by electrons passing through cell $S(x,y,z)$ is calculated as

$$N_{K\alpha}(S,D) = \int N_h(E,S)n_{gen}(E)f_{em}(S,D)dE, \quad (4)$$

where $N_h(E,S)$ is the number of electrons with energy E passing through cell S. $n_{\mathrm{gen}}(E)$ is the number of $K\alpha$ photons generated in S by an electron with energy E, which is determined by the K-shell cross section, cited from Ref. [26], and the fluorescence rate, cited from Ref. [27]. $f_{em}(S,D)$ is the rate of $K\alpha$ photon emission from S to D, which is determined by the absorption rate of x ray by the material, cited in Ref. [27].

To calculate $N_h(E,S)$, one needs to determine the energy of HE when transporting through the cell S, i.e., to consider the energy loss for HEs during transport. The contributions due to bremsstrahlung radiation as well as collisional ionization and excitation can be described by the stopping power [28]. The results are shown in the next section. Besides HE interaction with the material atoms, the static electric field E and magnetic field B produced by the electron current within the target lead to a return current and impact HE transport. In the calculation model we ignore the static electric and magnetic fields E and B, and as a complementarity, the magnitudes of E and B are discussed in next section.

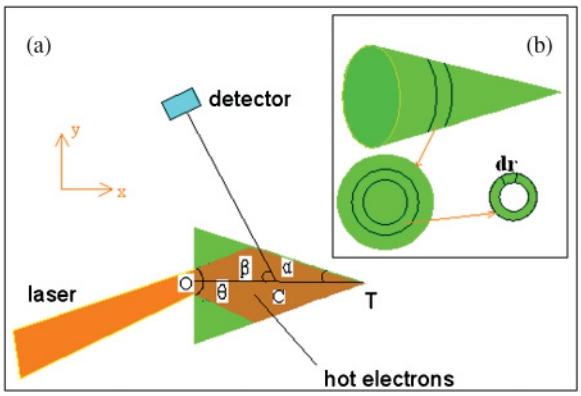

FIG. 1. (Color online) (a) Section-plane map of the model. O is the center of the underside, C is the axis midpoint, T is the cone tip, OT is the cone height, α is the cone angle, and θ is the HE divergence angle. The detector is 1 mm from C and crosses the axis at an angle β, which is varied from 0° to 180°. (b) Cell divisions in the cone.

III. THE RESULTS

The $K\alpha$ number density $n_{K\alpha}(\beta)$ detected at angle β is calculated as

$$n_{K\alpha}(\beta) = \sum_S N_{K\alpha}(S,D)/\mathrm{area}(D), \quad (5)$$

where area$(D) = 1\ \mu$m^2 and rotational symmetry around the cone axes is assumed. The results from cones and foils for HE temperatures of 40, 100, 200, and 300 keV are shown in Fig. 2, where the total energy of HEs has been normalized to 1 J. Obviously, $K\alpha$ radiation from cones is emitted over a wider angle and the photon density is much higher, which means a higher conversion efficiency from HE energy to $K\alpha$ photons. Photon emission from cones exhibits a peak at 180° that is at least twofold higher than the maximum emission at the foil rear side.

In the following we consider the photon density measured at 180° and the conversion efficiency ϵ_{HK} of HE energy to $K\alpha$ radiation, which is calculated as

$$\epsilon_{HK} = \frac{E_{K\alpha}\int n_{K\alpha}(\beta)2\pi\sin(\beta)L^2d\beta}{N_h^{\mathrm{tot}}\int f(E)EdE}, \quad (6)$$

where N_h^{tot} is the total number of HEs. To investigate the dependence of $K\alpha$ emission on the shape of the cone, the cone

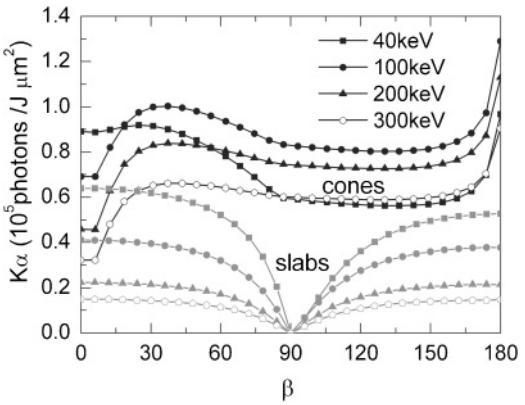

FIG. 2. $K\alpha$ photon density per joule of total HE energy measured at angles from 0° to 180° for different HE temperatures. Cone angle, 5° and height, 200 μm; foil thickness, 15 μm; HE divergence angle, 0°.

angle α was varied from 5° to 45° and the cone height from 50 to 500 μm for a HE temperature of 100 keV. The results in Fig. 3 indicate that ϵ_{HK} is higher for cones with a smaller angle, whereas the photon density at 180° favors a larger cone angle. This is reasonable because for sharp-angled cones, the distance the $K\alpha$ photons travel inside the cone is smaller, which avails the emission of x-ray photons. However, when the detector is at 180°, a wide-angle cone permits more photons to reach the detector. Thus when measuring large-scale targets, a sharp-angled cone would be better because it produces a higher number of x-ray photons. When a pointlike x-ray source is required, a wide-angle cone would be better because the emission exhibits a peak at the tip side.

According to the results in Fig. 3, only cones with an angle of 5° need to be considered for investigation of the conversion efficiency under optimal conditions, and a cone angle of 45° should be used when $K\alpha$ emission at 180° is investigated. Figures 4(a) and 4(b) show the dependence of $K\alpha$ emission on the cone height for different HE temperatures and a divergence angle of 0°. Results for foils are shown in Figs. 4(c) and 4(d) for comparison, which is consistent with the analytical model results [11], just that the target there is considered to be Ti, not copper. The optimal HE temperature for cones is higher than that for foils, because the cones decrease the reabsorption of x-ray photons, leading to higher conversion efficiency and maximum photon density when a suitable shape is chosen. The results for electron impact at a cone divergence angle of 20° [Figs. 5(a) and 5(b)] are lower than those at 0° [Figs. 4(a) and 4(b)], but they are still higher than those for foils [Figs. 4(c) and 4(d)].

The conversion efficiency of laser energy to $K\alpha$ radiation is calculated as

$$\epsilon_{LK} = \frac{E_{K\alpha} N_{K\alpha}^{\mathrm{tot}}}{E_{\mathrm{laser}}} = \epsilon_{HK} f_{\mathrm{abs}}, \tag{7}$$

where $N_{K\alpha}^{\mathrm{tot}}$ is the total number of $K\alpha$ photons, and f_{abs} is the absorption efficiency of HEs to the laser energy, which varies in a wide range according to laser pulse parameters and the plasma conditions [6,7,20,29,30]. In our calculation, f_{abs} is assumed to be 0.3. The results for $K\alpha$ emission dependence on laser intensity for foils and solid cones are shown in Fig. 6. The curve for the foil target can be compared with the particle-in-cell and Monte Carlo (PIC-MC) calculation in Ref. [10]. The difference comes from the fact that in Ref. [10] the HE temperature is considered proportional to $I^{1/2}$, and the number of HEs scale with I,

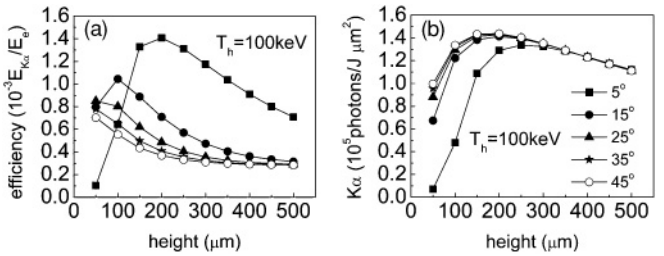

FIG. 3. (a) Efficiency of conversion from HE energy to $K\alpha$ photons and (b) photon density per joule of total HE energy detected at 180° for cone angles α of 5°, 15°, 25°, and 35° and a HE temperature of 100 keV. HE divergence angle, 0°.

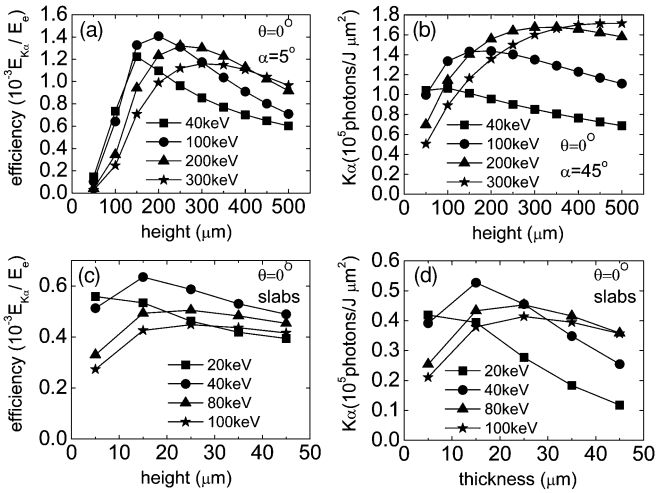

FIG. 4. (a) Conversion efficiency of HE energy to $K\alpha$ radiation and (b) photons per joule total HE energy emitted at 180° vs. cone height for different HE temperatures. The divergence angle of HE current is 0°. The corresponding results for foils are shown in (c) and (d).

while in our calculation the $T_h \sim I$ relation scales as Eqs. (2) and (3).

In summary, the above results indicate that for the HEs produced by femtosecond lasers, transport in cones would result in enhanced $K\alpha$ emission compared to foil targets. The maximum conversion efficiency of laser energy to $K\alpha$ emission for solid cones is 2 times higher than that for foils. For 1 J of laser energy, the maximum photon number density detected at the rear side for solid cones is 3 times higher than that for foils. Meanwhile, the optimal laser intensity for solid cones is at least 1 order of magnitude higher than that for foils. However, the calculation is based on a model in which the influence of electric and magnetic fields to HE transport is ignored and the contribution from return current to $K\alpha$ emission is neglected. In the next section, the electric and magnetic fields are estimated and their contribution to HE transport and $K\alpha$ emission in solid cones and foils is discussed.

IV. CONTRIBUTIONS FROM STATIC ELECTRIC AND MAGNETIC FIELDS

During HE transport, static electric and magnetic fields are generated inside the target and at the rear side surface. These

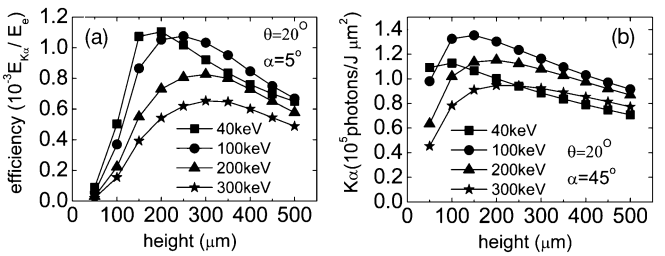

FIG. 5. (a) Conversion efficiency of HE energy to $K\alpha$ radiation and (b) photons per joule total HE energy emitted at 180° vs cone height for different HE temperatures. The divergence angle of HE current is 20°.

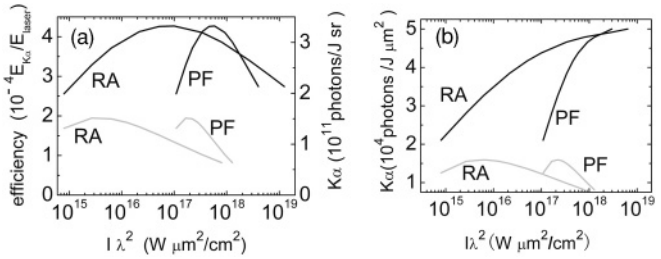

FIG. 6. (a) Conversion efficiency of laser energy to $K\alpha$ radiation and (b) photons per joule laser energy emitted at 180° vs laser intensity for solid cones (black lines) and foils (gray lines) when resonance absorption (RA) or ponderomotive force (PF) dominates.

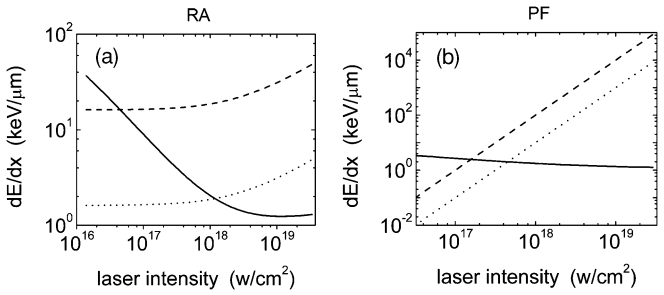

FIG. 7. Electric force (dashed lines for $\eta = 10^{-6}$ Ωm, dotted lines for $\eta = 10^{-7}$ Ωm) compared to stopping power (solid line) when resonant absorption (RA) or ponderomotive force (PF) dominates.

fields would affect the HE transport and have contributions to $K\alpha$ generation [31–33].

Electric and magnetic fields inside the target generated by the beam of HEs can be estimated according to Ref. [31] as

$$E = \eta j_c, \qquad \frac{\partial B}{\partial t} = -\nabla \times \eta j_c, \tag{8}$$

where η is the resistivity of the conductor, determined by the background temperature, and j_c is the current inside the conductor, which is generated over a time scale of $\tau_0 = \epsilon_0 \eta$ to balance the HE current j_h. For conductors with small resistivity, τ_0 is extremely rapid. Assuming a normal incident electron beam generated by a laser with intensity I, focus diameter d, and duration τ, the maximum value of the electric field can be approximately calculated as [31]

$$E_{\max} = \eta f_{\text{abs}} I / T_h, \tag{9}$$

where the HE temperature T_h is the average energy of relativistic HEs, and the electric force induced by $E_{\max}$ equals $eE_{\max}$. To calculate magnetic field, one needs to consider the space derivative of j_c and η according to Eq. (8). The results in Ref. [31] indicate that the value of the magnetic field is proportional to the laser duration and that the ratio of the forces on electrons induced by the electric and magnetic fields is

$$\frac{vB}{E} = 12\left(\frac{2\tau}{ps}\right)\left(\frac{10\,\mu\text{m}}{d/2}\right)\left(\frac{v}{c}\right). \tag{10}$$

We estimate the force induced by electric fields only in the calculation, keeping in mind that the magnetic field increases with the increase of the electric field. The results for electric force compared with stopping power are shown in Fig. 7, where HEs are considered as a monoenergetic beam with energy T_h related to laser intensity I when resonance absorption (RA) or ponderomotive force (PF) dominates. The resistivity is considered to be 10^{-6} and 10^{-7} Ωm, corresponding to background temperature of the order of electronvolts and tens of electronvolts. The background temperature of targets heated by HEs is hard to measure. In Ref. [34], the temperature of aluminum irradiated under a 10-J, 150-fs laser is measured to be 10 eV, corresponding to resistivity 10^{-6} Ωm [31]. Considering that for a femtosecond laser with total energy around 1 J, the HEs generated would have a total energy much lower, the temperature of background heated by HEs would therefore be lower. Besides, the resistivity of copper is smaller than aluminum. We consider the resistivity of the copper background as larger than 10^{-7} Ωm but much lower than $\sim 10^{-6}$ Ωm. Upon comparing Fig. 7 with Fig. 6, it is easy to see that for foils, the electric field is not a major effect when optimal condition of laser intensity is considered. For solid cones, the optimal laser intensity for total efficiency is 10^{17} W/cm^2 when resonance absorption dominates, and the static electric forces do not play a central role. However, when ponderomotive force dominates or when the optimal condition for x-ray intensity at the rear side is considered, the static electric fields become important.

The static electric field inside the target would accelerate background electrons and produce a return current directed to the underside of the cone. For a laser pulse with half duration 50 fs, the HE beam would be generated within 100 fs. For HEs with temperatures of 100 keV, the major part of the beam has a length of approximately 20 μm. The reflected electrons have an energy of

$$\varepsilon_{\text{refl}} = \varepsilon_0 + \int \vec{f}_E(t) \cdot \vec{v} dt, \tag{11}$$

where $\vec{f}_E$ is the electric force induced by HE current, and ε_0 is the initial energy of the electron, which can be assumed to be neglectable. In approximation, the value of $\varepsilon_{\text{refl}}$ is calculated as $f_E \times 20\ \mu$m, which equals 20 keV if $f_E = 1$ keV/μm (as high as the stopping power) corresponds to the optimal electron energy for K-shell impact ionization. Therefore, although the present of static electric and magnetic fields reduces the energy of HEs and the efficiency of $K\alpha$ generation as indicated in Ref. [32], the electrons accelerated by the electric fields have a contribution to $K\alpha$ x-ray generation and increase the efficiency of $K\alpha$ generation. As the accelerated electrons have energy around 20 keV, a proper control of HE transport would result in further improvement of $K\alpha$ emission.

For reflected electrons with energy 20 keV generated 10 μm away from the target surface, it needs a time of 100 fs to reach the underside of the cone. So only the reflexing generated nearer than 10 μm away from the target surface would be concerned with laser-plasma interaction. HE production can be considered to be unaltered by the return current.

Now we discuss the electric fields at the surface of the target. For foils, electric fields at the rear side surface are generated by spray of energetic electrons, i.e., high-energy electrons with

energy larger than 1 MeV [35,36]. A reflexing induced by that electric field would be concerned with surface laser-plasma interaction. However, for solid cones with a height several hundreds of micrometers, it take a longer time for energetic electrons generated at the underside of the cone to reach the cone surface and the electron energy is reduced by the stopping power. Meanwhile, the density of energetic electrons at the surface of a solid cone is much smaller than that at the rear surface of foils. Thereby, the electric fields at the surface of a solid cone would be much smaller and the reflexing would be much weaker, and it takes a much longer time than the duration of the laser for the reflexing to reach the underside of the cone. Therefore, no reflexing is concerned with laser-plasma interaction for femtosecond laser irradiation of solid cone targets. However, a prominent electric field would be generated at the cone tip, which would prevent energetic electrons from leaving the cone but cause an acceleration of ions. To prevent ion acceleration, one can cut off the tip of the cone.

V. CONCLUSION

In this work, the possibility of improving $K\alpha$ emission through femtosecond laser irradiation of a solid cone target is studied theoretically. According to the model for HE transport and $K\alpha$ generation, where contributions from static electric and magnetic fields in the target have been ignored, solid cones have an advantage over foils from which the $K\alpha$ photons emit in a wider space angle, the conversion efficiency from electron energy to $K\alpha$ x ray energy is much larger, and the optimal laser intensity is much higher. Therefore, the maximum $K\alpha$ emission one could obtain from solid cone targets would be several times higher than that from foil targets. Based on an approximate estimation, the electric and magnetic fields generated by HEs in solid cones is discussed. When resonance absorption dominates during laser-plasma interaction, the static electric fields inside the target do not play an important role. When the laser intensity is further increased or when ponderomotive force dominates, the static electric fields become important. Return current accelerated by the inside static electric fields and the reflexing generated by spray of energetic electrons would have a contribution to $K\alpha$ generation. An explicit calculation of the contributions from static electric and magnetic fields would give us further understanding of HE transport and $K\alpha$ emission from solid cones.

ACKNOWLEDGMENT

We have benefited greatly from discussions with Fu-Qian Jing and Jian-Feng Li. This work is supported in part by the National Natural Science Foundation of China (under Grant No. 10974056).

[1] B. Barbrel, M. Koenig, A. Benuzzi-Mounaix, E. Brambrink, C. R. D. Brown, D. O. Gericke, B. Nagler, M. Rabec le Gloahec, D. Riley, C. Spindloe *et al.*, Phys. Rev. Lett. **102**, 165004 (2009).

[2] E. G. Saiz, G. Gregori, D. O. Gericke, J. Vorberger, B. Barbrel, R. J. Clarke, R. R. Freeman, S. H. Glenzer, F. Y. Khattak, M. Koenig *et al.*, Nature Physics **4**, 940 (2008).

[3] D. Riley, N. C. Woolsey, D. McSherry, I. Weaver, A. Djaoui, and E. Nardi, Phys. Rev. Lett. **84**, 1704 (2000).

[4] B. X. Hou, J. A. Nees, W. Theobald, G. A. Mourou, L. M. Chen, J. C. Kieffer, A. Krol, and C. C. Chamberlain, Appl. Phys. Lett. **84**, 2259 (2004).

[5] W. Lu, M. Nicoul, U. Shymanovich, A. Tarasevitch, P. Zhou, K. Sokolowski-Tinten, D. von der Linde, M. Mašek, P. Gibbon, and U. Teubner, Phys. Rev. E **80**, 26404 (2009).

[6] P. P. Rajeev, S. Banerjee, A. S. Sandhu, R. C. Issac, L. C. Tribedi, and G. R. Kumar, Phys. Rev. A **65**, 52903 (2002).

[7] L. Cao, Y. Gu, Z. Zhao, L. Cao, W. Huang, W. Zhou, X. He, W. Yu, and M. Yu, Phys. Plasmas **17**, 043103 (2010).

[8] C. A. Back, J. Grun, C. Decker, L. J. Suter, J. Davis, O. L. Landen, R. Wallace, W. W. Hsing, J. M. Laming, U. Feldman, M. C. Miller, and C. Wuest, Phys. Rev. Lett. **87**, 275003 (2001).

[9] K. B. Fournier, C. Constantin, J. Poco, M. C. Miller, C. A. Back, L. J. Suter, J. Satcher, J. Davis, and J. Grun, Phys. Rev. Lett. **92**, 165005 (2004).

[10] C. Reich, P. Gibbon, I. Uschmann, and E. Förster, Phys. Rev. Lett. **84**, 4846 (2000).

[11] D. Salzmann, C. Reich, I. Uschmann, E. Förster, and P. Gibbon, Phys. Rev. E **65**, 36402 (2002).

[12] F. Y. Khattak, O. A. M. B. PercieduSert, D. Riley, P. S. Foster, E. J. Divall, C. J. Hooker, A. J. Langley, J. Smith, and P. Gibbon, Phys. Rev. E **74**, 27401 (2006).

[13] D. C. Eder, G. Pretzler, E. Fill, K. Eidmann, and A. Saemann, Appl. Phys. B **70**, 211 (2000).

[14] L. Van Woerkom, K. U. Akli, T. Bartal, F. N. Beg, S. Chawla, C. D. Chen, E. Chowdhury, R. R. Freeman, D. Hey, M. H. Key *et al.*, Phys. Plasmas **15**, 056304 (2008).

[15] R. J. Mason, Phys. Rev. Lett. **96**, 35001 (2006).

[16] B. I. Cho, G. M. Dyer, S. Kneip, S. Pikuz, D. R. Symes, A. C. Bernstein, Y. Sentoku, N. Renard-Le Galloudec, T. E. Cowan, and T. Ditmire, Phys. Plasmas **15**, 052701 (2008).

[17] C. Reich, I. Uschmann, F. Ewald, S. Düsterer, A. Lübcke, H. Schwoerer, R. Sauerbrey, E. Förster, and P. Gibbon, Phys. Rev. E **68**, 56408 (2003).

[18] J. A. Halbleib, R. P. Kensek, T. A. Mehlhorn, G. D. Valdez, S. M. Seitzer, and M. J. Berger, ITS Version 3—The Integrated TIGER Series of Coupled Electron/Photon Monte Carlo Transport Codes, Sandia National Laboratories (unpublished).

[19] B. C. Franke, R. P. Kensek, and T. W. Laub, ITS Version 5.0—The Integrated TIGER Series of Coupled Electron/Photon Monte Carlo Transport Codes with CAD Geometry, Sandia National Laboratories, Tech. Rep. SAND2004-5172, 2005.

[20] G. Malka and J. L. Miquel, Phys. Rev. Lett. **77**, 75 (1996).

[21] Y. Okano, Y. Hironaka, K. G. Nakamura, K. Kondo, Y. Oishi, T. Nayuki, and K. Nemoto, J. Appl. Phys. **95**, 2278 (2004).

[22] K. B. Wharton, S. P. Hatchett, S. C. Wilks, M. H. Key, J. D. Moody, V. Yanovsky, A. A. Offenberger, B. A. Hammel, M. D. Perry, and C. Joshi *et al.*, Phys. Rev. Lett. **81**, 822 (1998).

[23] F. N. Beg, A. R. Bell, A. E. Dangor, C. N. Danson, A. P. Fews, M. E. Glinsky, B. A. Hammel, P. Lee, P. A. Norreys, and M. Tatarakis, Phys. Plasmas **4**, 447 (1997).
[24] S. C. Wilks and W. L. Kruer, IEEE J. Quantum Electron. **33**, 1954 (1997).
[25] Z. M. Sheng, Y. Sentoku, K. Mima, J. Zhang, W. Yu, and J. Meyer-ter-Vehn, Phys. Rev. Lett. **85**, 5340 (2000).
[26] C. Hombourger, J. Phys. B **31**, 3693 (1998).
[27] Mucal on the web [http://csrri.iit.edu/mucal.htm].
[28] J. Turner, *Atoms, Radiation, and Radiation Protection* (VCH Publishers, New York, 2007).
[29] M. Cerchez, R. Jung, J. Osterholz, T. Toncian, O. Willi, P. Mulser, and H. Ruhl, Phys. Rev. Lett. **100**, 245001 (2008).
[30] H. Cai, W. Yu, S. Zhu, C. Zheng, L. Cao, B. Li, Z. Chen, and A. Bogerts, Phys. Plasmas **13**, 094504 (2006).
[31] J. R. Davies, A. R. Bell, M. G. Haines, and S. M. Guerin, Phys. Rev. E **56**, 7193 (1997).
[32] J. R. Davies, Phys. Rev. E **65**, 26407 (2002).
[33] J. R. Davies, Phys. Rev. E **68**, 56404 (2003).
[34] E. Martinolli, M. Koenig, F. Amiranoff, S. D. Baton, L. Gremillet, J. J. Santos, T. A. Hall, M. Rabec-Le-Gloahec, C. Rousseaux, and D. Batani, Phys. Rev. E **70**, 0055402 (2004).
[35] H. S. Park, N. Izumi, M. H. Key, J. A. King, J. A. Koch, O. L. Landen *et al*., Phys. Plasmas, UCRL (2005).
[36] A. J. Mackinnon, Y. Sentoku, P. K. Patel, D. W. Price, S. Hatchett, M. H. Key, C. Andersen, R. Snavely, and R. R. Freeman, Phys. Rev. Lett. **88**, 215006 (2002).